ISSN 1070-3284, Russian Journal of Coordination Chemistry, 2023, Vol. 49, No. 3, pp. 124–141. © Pleiades Publishing, Ltd., 2023.
Russian Text © The Author(s), 2023, published in Koordinatsionnaya Khimiya, 2023, Vol. 49, No. 3, pp. 138–156.

Complexes $R_2Sn(IV)L$ with O,N,O'-Donor Schiff Bases: Synthesis, Structures, and Redox Properties

I. V. Smolyaninov[a], *, D. A. Burmistrova[a], N. P. Pomortseva[a], Yu. K. Voronina[b], A. I. Poddel'sky[c], N. T. Berberova[a], and I. L. Eremenko[b]

[a] *Astrakhan State Technical University, Astrakhan, Russia*

[b] *Kurnakov Institute of General and Inorganic Chemistry, Russian Academy of Sciences, Moscow, Russia*

[c] *Razuvaev Institute of Organometallic Chemistry, Russian Academy of Sciences, Nizhny Novgorod, Russia*

**e-mail: ivsmolyaninov@gmail.com*

Received July 1, 2022; revised August 17, 2022; accepted August 23, 2022

Abstract—New tin(IV) complexes with O,N,O'-donor Schiff bases (L^1H_2–L^4H_2) of the (L^n)SnR_2 type (R = Ph (**I**–**III**), Et (**IV**–**VII**)) are synthesized and characterized. The molecular structures of compounds **I**–**III**, **VI**, and **VII** in the crystalline form are determined by X-ray diffraction (XRD) (CIF files CCDC nos. 2181140 (**I**), 2181142 (**II**), 2181143 (**III**·CH_3CN), 2181141 (**VI**), and 2181139 (**VII**)). Tin complexes **I**–**III** and **VI** are mononuclear pentacoordinate compounds. Crystalline complex **VII** forms dimers via the pairwise bridging coupling between the oxygen and tin atoms of the mononuclear fragments. The redox-active ligand in the synthesized compounds exists as the iminobis(phenolate) dianion. The electrochemical properties of free ligands and complexes **I**–**VII** are studied. In the case of compounds **I**, **II**, **IV**, and **V** with *tert*-butyl substituents in the redox-active ligand, the formation of relatively stable monocationic and monoanionic species is electrochemically detected for the first time. The presence of the electroactive nitro group results in the destabilization of the oxidized forms of the complexes and induces the appearance of an additional peak in the cathodic range. The energy gaps between the frontier redox orbitals are determined by the electrochemical and spectral methods. The obtained parameters are close and vary in a range of 2.43–2.68 eV.

Keywords: tin(IV) complexes, redox-active Schiff bases, XRD, cyclic voltammetry, redox transformations

DOI: 10.1134/S1070328423700446

INTRODUCTION

A rational design of new complexes and a comprehensive study of their properties presently form a basis for the search and revealing platform compounds used in the fabrication of useful materials. Schiff bases refer to simple and available ligands for the synthesis of multicenter molecules. The compounds of a similar type containing redox-active phenol, catechol, and ferrocenyl fragments and their combinations are characterized by a pronounced biological activity [1–3] and are widely used in coordination chemistry [4–7]. The complexes based on ligands of this class find use in catalysis [8, 9] and in the chemistry of functional materials with useful mechanical, thermal, chemical, or optoelectronic properties [10–12]. From the viewpoint of medical and pharmaceutical chemistry, these compounds attract attention as antiviral, antifungal, antimicrobial, antituberculous, and antitumor agents [13–16].

The tin(II/IV) compounds bearing the redox-active ligands [17–20] can be considered as potential components in molecular electronics and spintronics and as a basis for manufacturing lithium current sources, solar cells, and magnetoactive materials. The ability of redox-active ligands to reversibly change the oxidation state being in the coordination sphere of the metal are of special interest for the chemistry of several nontransition metal derivatives. This is related to the fact that these metals, as a rule, have no many accessible redox states.

The application of O,N,O'-donor Schiff bases in combination with organometallic tin(IV) derivatives leads to the formation of complexes capable of increasing the number of accessible redox forms due to a change in the oxidation/reduction state of the ligand. A distinctive feature of these complexes is no necessity of involving the metal, since the ligand can act as an electron reservoir, which makes it possible to extend boundaries of using metals of the main subgroups. The disubstituted organic tin(IV) derivatives turned out to be chelating sites with appropriate sizes for the tridentate Schiff bases based on salicylaldehyde. Objects of a similar type can be used as easily tunable polychromic systems, which can be fairly labile due to the variation of substituents in aromatic rings of the ligand or organic groups at the tin(IV) atom [21]. This approach

finds use in the synthesis of the compounds characterized by luminescence (fluorescent) activity [22].

Along with the specific optical properties, the tin(IV) complexes with the Schiff bases are referred to promising objects in inorganic medical chemistry due to their antimicrobial, antiproliferative, and antitumor activities [23–25]. The biological properties can be modulated due to a combination of the organotin fragment with the Schiff bases bearing antioxidant phenol groups, which results in a balance of the antioxidant protector function and cytotoxicity [26]. An analysis of the published data revealed many tin(IV) compounds containing the tridentate O,N,O'-donor Schiff bases [27–34]. There are no complexes with Schiff bases bearing sterically hindered *tert*-butyl groups and electron-withdrawing substituents in aromatic rings among the compounds described in the literature. Therefore, the purpose of this work is the synthesis of new tin(IV) complexes with redox-active O,N,O'-donor Schiff bases and study of their structures and electrochemical and spectral properties. Ligands L^1H_2–L^4H_2 used in the work and synthesized by the condensation of 3,5-di-*tert*-butyl-2-hydroxybenzaldehyde with *o*-aminophenols can react with the organometallic tin(IV) derivatives to form stable complexes. The presence of substituents stabilizing different redox states in the ligand makes it possible to use electrochemical methods for the detection of oxidized/reduced forms of the complexes, estimation of their stability, and determination of the energy gap between the frontier redox orbitals.

The purposes of this work are to synthesize new tin(IV) complexes with the O,N,O'-donor Schiff bases (L^1H_2–L^4H_2) of the (L^n)SnR_2 type (R = Ph (**I**–**III**), Et (**IV**–**VII**)), to determine their molecular structures, to study electrochemical transformations of the free ligands and complexes, to examine spectral properties, and to estimate the energy gap between the frontier redox orbitals.

EXPERIMENTAL

Commercial reagents Ph_2SnCl_2 (Aldrich, 96%), Et_2SnCl_2 (Aldrich, 98%), 3,5-di-*tert*-butylsalicylaldehyde (Acros Organics, 99%), 2-amino-4-*tert*-butylphenol (Alfa Aesar, 97%), 2-amino-4-chloro-6-nitrophenol (Aldrich, 97%), 6-amino-2,4-dichloro-3-methylphenol hydrochloride (Fluka, 97%), and tetra-*n*-butylammonium perchlorate (Bu_4NClO_4) (Alfa Aesar, 99%) were used as received. 4,6-Di-*tert*-butyl-*o*-aminophenol was synthesized using a known procedure [35]. The solvents used in the work were purified and dehydrated using standard procedures [36].

^1H and ^{13}C NMR spectra were recorded on a Bruker AVANCE HD 400 spectrometer with a frequency of 400 MHz (^1H) and 100 NHz (^{13}C) using tetramethylsilane as the internal standard and $CDCl_3$ as the solvent. IR spectra were recorded on an FSM 1201 FT-IR spectrometer in KBr pellets in a range of 400–4000 cm^{-1}. High resolution mass spectra were measured on a Bruker UHR-TOF Maxis™ mass spectrometer (ESI). Elemental analysis was carried out on a Euro EA 3000 (C,H,N) analyzer. Absorption spectra were recorded on an SF-104 spectrophotometer in a range of 300–600 nm at room temperature. Electrochemical potentials of the studied compounds were measured by cyclic voltammetry (CV) in a three-electrode cell on an IPC-pro potentiostat in acetonitrile under argon. A stationary glassy carbon (GC) electrode with a diameter of 2 mm served as the working electrode, and a platinum plate ($S = 18$ mm^2) served as the auxiliary electrode. The reference electrode (Ag/AgCl/KCl) with a waterproof membrane was used. The concentration of the compounds was 0.003 mol/L. The number of electrons transferred during the electrode process was estimated relative to ferrocene used as the standard. The potential sweep rate was 0.2 $V\,s^{-1}$. The supporting electrolyte was 0.1 M *n*-Bu_4NClO_4.

Microelectrolysis of L^1H_2, L^2H_2, and complex **VI** was carried out using a VersaSTAT potentiostat at stationary platinum electrodes (plates with a surface area of 30 mm^2) in a 2-mL undivided three-electrode cell at a potential of 1.15–1.4 V (electrolysis time 1.5 h). An electrode with an electroconducting waterproof membrane (Ag/AgCl/KCl) was used as the reference electrode. Ligands L^2H_2 (MeCN) or L^1H_2 and complex **VI** (CH_2Cl_2) were added to a predeaerated electrochemical cell containing a solution of the supporting electrolyte (0.1 M *n*-Bu_4NClO_4). The concentration of the studied compound in the electrochemical cell was 0.003 mol/L.

Synthesis of Schiff bases L^1H_2–L^4H_2 was carried out by the reactions of 3,5-di-*tert*-butylsalicylaldehyde (4 mmol) with the corresponding *o*-aminophenols (4 mmol) in methanol (20 mL). A solution of *o*-aminophenol was added dropwise to a solution of benzaldehyde for 30 min, and then the resulting solution was refluxed under an inert gas (argon) for 5 h. The solution was slowly cooled to room temperature. The formed precipitate was filtered off and dried in vacuo.

2,4-Di-*tert*-butyl-6-((((5-*tert*-butyl)-2-hydroxyphenyl)imino)methyl)phenol (L^1H_2). The yield was 0.83 g (2.2 mmol, 55%).

IR (KBr; ν, cm^{-1}): 3529, 3060, 2964, 2910, 2870, 1615, 1581, 1500, 1469, 1435, 1392, 1364, 1326, 1270, 1249, 1218, 1202. ^1H NMR ($CDCl_3$; 400 MHz; δ, ppm): 1.36 (s, 9H, *t*-Bu), 1.37 (s, 9H, *t*-Bu), 1.49 (s, 9H, *t*-Bu), 5.71 (br.s, 1H, OH), 6.97 (d, $^3J_{H,H}$ = 8.5 Hz, 1H, arom. C_6H_3), 7.15 (d, $^4J_{H,H}$ = 2.1 Hz, 1H, arom. C_6H_3), 7.25 (dd, $^3J_{H,H}$ = 8.5 Hz, $^4J_{H,H}$ = 2.1 Hz, 1H, arom. C_6H_3), 7.31 (d, $^4J_{H,H}$ = 2.2 Hz, 1H, arom. C_6H_2), 7.51 (d, $^4J_{H,H}$ = 2.2 Hz, 1H, arom. C_6H_2), 8.72 (s, 1H, CH=N), 12.98 (br.s, 1H, OH). ^{13}C NMR

($CDCl_3$; 100 MHz; δ, ppm): 29.40, 31.45, 31.55, 34.23, 34.38, 35.10, 115.07, 115.23, 118.50, 125.32, 127.20, 128.59, 135.20, 137.09, 141.12, 144.00, 147.41, 157.73, 164.83.

Found, *m/z*: 380.2599 $[M]^+$. For $C_{25}H_{34}NO_2$ calculated, *m/z*: 380.2595.

2,4-Di-*tert*-butyl-6-((3,5-di-*tert*-butyl-2-hydroxybenzelidene)amino)phenol (L^2H_2). The yield was 1.10 g (2.5 mmol, 62%).

IR (KBr; ν, cm^{-1}): 3519, 3458, 2957, 2907, 2866, 1615, 1584, 1481, 1468, 1440, 1413, 1392, 1361, 1331, 1271, 1250, 1219, 1200. ^1H NMR (400 MHz; $CDCl_3$; δ, ppm): 1.35 (s, 9H, *t*-Bu), 1.36 (s, 9H, *t*-Bu), 1.46 (s, 9H, *t*-Bu), 1.48 (s, 9H, *t*-Bu), 6.23 (br.s, 1H, OH), 7.02 (d, $^4J_{H,H}$ = 2.1 Hz, 1H, arom. C_6H_2), 7.28 (d, $^4J_{H,H}$ = 2.1 Hz, 1H, arom. C_6H_2), 7.30 (d, $^4J_{H,H}$ = 2.3 Hz, 1H, arom. C_6H_2), 7.50 (d, $^4J_{H,H}$ = 2.3 Hz, 1H, arom. C_6H_2), 8.70 (s, 1H, CH=N), 12.69 (br.s, 1H, OH). ^{13}C NMR (100 MHz; $CDCl_3$; δ, ppm): 29.40, 29.50, 31.45, 31.62, 34.25, 34.59, 35.05, 35.71, 112.66, 118.63, 123.01, 127.27, 128.70, 135.39, 135.77, 137.25, 141.30, 142.47, 146.12, 157.55, 164.63.

Found, *m/z*: 438.3358 $[M + H]^+$. For $C_{29}H_{44}NO_2$ calculated, *m/z*: 438.3367.

2,4-Di-*tert*-butyl-6-(((5-chloro-2-hydroxy-3-nitrophenyl)imino)methyl)phenol (L^3H_2). The yield was 1.14 g (2.8 mmol, 62%).

IR (KBr; ν, cm^{-1}): 3225, 3082, 2961, 2910, 2870, 1620, 1597, 1580, 1522, 1470, 1435, 1408, 1363, 1310, 1248, 1202. ^1H NMR (400 MHz; $CDCl_3$; δ, ppm): 1.33 (s, 9H, *t*-Bu), 1.48 (s, 9H, *t*-Bu), 7.24 (d, $^4J_{H,H}$ = 2.4 Hz, 1H, arom. C_6H_2), 7.47 (d, $^4J_{H,H}$ = 2.5 Hz, 1H, arom. C_6H_2), 7.52 (d, ^4J(H,H) = 2.4 Hz, 1H, arom. C_6H_2), 8.01 (d, $^4J_{H,H}$ = 2.5 Hz, 1H, arom. C_6H_2), 8.74 (s, 1H, CH=N), 10.87 (s, 1H, OH), 13.24 (br.s, 1H, OH). ^{13}C NMR (100 MHz; $CDCl_3$; δ, ppm): 29.38, 31.39, 34.20, 35.16, 117.90, 121.24, 124.88, 127.18, 127.26, 129.51, 134.25, 137.48, 140.83, 140.99, 148.11, 158.86, 166.65.

Found, %: C, 62.18; H, 6.47; N, 7.01. For $C_{21}H_{25}ClN_2O_4$ calculated, %: C, 62.30; H, 6.22; N, 6.92.

2,4-Di-chloro-6-((3,5-di-*tert*-butyl-2-hydroxybenzelidene)amino)-3-methylphenol (L^4H_2). The yield was 1.14 g (2.8 mmol, 70%).

IR (KBr; ν, cm^{-1}): 3515, 3532, 3008, 2961, 2910, 2869, 1613, 1580, 1470, 1434, 1395, 1373, 1361, 1334, 1295, 1273, 1251, 1229, 1202. ^1H NMR (400 MHz; $CDCl_3$; δ, ppm): 1.33 (s, 9H, *t*-Bu), 1.47 (s, 9H, *t*-Bu), 2.48 (s, 3H, CH_3), 5.97 (br.s, 1H, OH), 7.17 (s, 1H, arom. C_6H_1), 7.24 (d, $^4J_{H,H}$ = 2.4 Hz, 1H, arom. C_6H_2), 7.49 (d, $^4J_{H,H}$ = 2.4 Hz, 1H, arom. C_6H_2), 8.70 (s, 1H, CH=N), 12.93 (br.s, 1H, OH). ^{13}C NMR (100 MHz; $CDCl_3$; δ, ppm): 17.69, 29.39, 31.41, 34.21, 35.12, 117.86, 118.18, 121.96, 125.95, 127.26, 129.03, 132.95, 134.62, 137.24, 141.08, 144.61, 158.21, 165.50.

Found, *m/z*: 408.1498 $[M + H]^+$. For $C_{22}H_{28}Cl_2NO_2$ calculated, *m/z*: 408.1492.

Synthesis of tin complexes (L)SnR_2 (I–VII). Compound R_2SnCl_2 (1 equiv, 0.3 mmol) in acetonitrile (2 mL) was added to a solution of Schiff base (0.3 mmol) in acetonitrile (3 mL), the solution was deaerated with argon for 5 min, and triethylamine (2 equiv) was added. The reaction medium turned orange-red upon the interaction of pale yellow solutions of the Schiff bases with the tin(IV) salts in the presence of the base. The resulting solution was left to stay at room temperature for 3 days. In the case of complexes **I**, **II**, **VI**, **V**, and **VII**, the formed crystalline precipitates were filtered off, washed with cold methanol, and dried in vacuo. For compounds **III** and **VI**, the reaction mixture was evaporated to 2 mL and cooled at 5°C for 24 h. The formed crystalline precipitates were filtered off, washed with cold methanol, and dried in vacuo.

(L^1)$SnPh_2$ (I). The yield of red-orange crystals was 0.094 g (48%). IR (KBr; ν, cm^{-1}): 3069, 3057, 2954, 2903, 2867, 1608, 1591, 1555, 1532, 1500, 1487, 1459, 1431, 1382, 1361, 1309, 1301, 1275, 1251, 1232, 1200.

^1H NMR (400 MHz; $CDCl_3$; δ, ppm): 1.36 (s, 18H, *t*-Bu), 1.54 (s, 9H, *t*-Bu), 7.03 (d, $^3J_{H,H}$ = 8.6 Hz, 1H, arom. C_6H_3), 7.12 (d, $^4J_{H,H}$ = 2.4 Hz, 1H, arom. C_6H_2), 7.29 (dd, $^3J_{H,H}$ = 8.6 Hz, $^4J_{H,H}$ = 2.1 Hz, 1H, arom. C_6H_3), 7.34 (d, $^4J_{H,H}$ = 2.1 Hz, 1H, arom. C_6H_3), 7.35–7.44 (m, 6H, arom. C_6H_5), 7.62 (d, $^4J_{H,H}$ = 2.4 Hz, 1H, arom. C_6H_2), 7.87–7.93 (m, 4H, arom. C_6H_5, with satellite splitting on tin nuclei, $^3J_{H,Sn}$ = 77 Hz), 8.72 (s, 1H, CH=N, with satellite splitting on tin nuclei, $^3J_{H,Sn}$ = 62.5 Hz). ^{13}C NMR (100 MHz; $CDCl_3$; δ, ppm): 29.90, 31.24, 31.62, 34.08, 34.32, 35.45, 110.90, 117.21, 117.95, 127.10, 128.50 (*J*(C,Sn) = 86.0/83.0 Hz), 129.53, 130.02 (*J*(C,Sn) = 17.2 Hz), 130.38, 132.42, 136.45 (*J*(C,Sn) = 55.4 Hz), 139.01, 139.55, 140.22, 140.94, 156.44, 162.14, 167.46.

Found, *m/z*: 654.2377 $[M + H]^+$. For $C_{37}H_{44}NO_2Sn$ calculated, *m/z*: 654.2396.

(L^2)$SnPh_2$ (II). The yield of orange crystals was 0.120 g (56%).

IR (KBr; ν, cm^{-1}): 3069, 3057, 2995, 2962, 2905, 2868, 1608, 1592, 1555, 1543, 1476, 1459, 1429, 1382, 1360, 1312, 1300, 1278, 1260, 1231, 1201.

^1H NMR (400 MHz; $CDCl_3$; δ, ppm): 1.36 (s, 18H, *t*-Bu), 1.55 (s, 9H, *t*-Bu), 1.56 (s, 9H, *t*-Bu), 7.10 (d, $^4J_{H,H}$ = 2.3 Hz, 1H, arom. C_6H_2), 7.23 (d, $^4J_{H,H}$ = 1.8 Hz, 1H, arom. C_6H_2), 7.31 (d, $^4J_{H,H}$ = 1.8 Hz, 1H, arom. C_6H_2), 7.33–7.44 (m, 6H, arom. C_6H_5), 7.61 (d,

$^4J_{H,H}$ = 2.3 Hz, 1H, arom. C_6H_2), 7.89–7.95 (m, 4H, arom. C_6H_5, with satellite splitting on tin nuclei, $^3J_{H,Sn}$ = 77 Hz), 8.67 (s, 1H, CH=N, with satellite splitting on tin nuclei, $^3J_{H,Sn}$ = 62.2 Hz). ^{13}C NMR (100 MHz, $CDCl_3$, δ, ppm): 29.60, 29.98, 31.28, 31.67, 34.08, 34.52, 35.29, 35.48, 108.72, 117.36, 123.98, 128.36 ($J_{C,Sn}$ = 85.2/82.2 Hz), 129.55, 129.87 ($J_{C,Sn}$ = 16.9 Hz), 130.31, 132.12, 136.52 ($J_{C,Sn}$ = 54.8 Hz), 137.97, 138.34, 138.89, 140.82, 140.88, 155.24, 162.27, 167.27.

Found, *m/z*: 710.2379 $[M + H]^+$. For $C_{41}H_{52}NO_2Sn$ calculated, *m/z*: 710.3023.

$(L^3)SnPh_2$ (III). The yield of red crystals was 0.100 g (50%).

IR (KBr; ν, cm^{-1}): 3053, 2963, 2907, 2868, 1612, 1588, 1556, 1523, 1460, 1432, 1423, 1403, 1389, 1344, 1315, 1252, 1221, 1200.

^1H NMR (400 MHz; $CDCl_3$; δ, ppm): 1.34 (s, 9H, *t*-Bu), 1.56 (s, 9H, *t*-Bu), 7.11 (d, $^4J_{H,H}$ = 2.5 Hz, 1H, arom. C_6H_2), 7.36–7.48 (m, 6H, arom. C_6H_5), 7.47 (d, $^4J_{H,H}$ = 2.5 Hz, 1H, arom. C_6H_2), 7.73 (d, $^4J_{H,H}$ = 2.5 Hz, 1H, arom. C_6H_2), 7.92 (d, $^4J_{H,H}$ = 2.5 Hz, 1H, arom. C_6H_2), 7.88–7.94 (m, 4H, arom. C_6H_5, with satellite splitting on tin nuclei, $^3J_{H,Sn}$ = 80.6 Hz), 8.66 (s, 1H, CH=N, with satellite splitting on tin nuclei, $^3J_{H,Sn}$ = 54.8 Hz). ^{13}C NMR (100 MHz; $CDCl_3$, δ, ppm): 29.91, 31.06, 34.15, 35.55, 117.14, 119.25, 119.51, 124.54, 128.95 ($J_{H,Sn}$ = 89.3/86.2 Hz), 130.25, 130.70 ($J_{C,Sn}$ = 17.6 Hz), 134.96, 136.25, 136.36 ($J_{C,Sn}$ = 57.8 Hz), 138.38, 138.45, 140.30, 141.54, 153.28, 165.15, 169.00.

Found, *m/z*: 699.1010 $[M + Na]^+$. For $C_{33}H_{33}ClN_2NaO_4Sn$ calculated, *m/z*: 699.1043.

$(L^1)SnEt_2$ (IV). The yield of a red-orange finely crystalline powder was 0.100 g (60%).

IR (KBr; ν, cm^{-1}): 3027, 2952, 2869, 1612, 1586, 1545, 1530, 1490, 1461, 1425, 1406, 1384, 1360, 1328, 1279, 1255, 1232, 1197.

^1H NMR (400 MHz; $CDCl_3$; δ, ppm): 1.27 (t, ^3J(H,H) = 7.9 Hz, 6H, Me), 1.33 (s, 9H, *t*-Bu), 1.35 (s, 9H, *t*-Bu), 1.31–1.36 (m, 4H, CH_2), 1.41 (s, 9H, *t*-Bu), 6.80 (d, $^3J_{H,H}$ = 8.6 Hz, 1H, arom. C_6H_3), 7.06 (d, $^4J_{H,H}$ = 2.5 Hz, 1H, arom. C_6H_2), 7.22 (dd, $^3J_{H,H}$ = 8.6 Hz, $^4J_{H,H}$ = 2.2 Hz, 1H, arom. C_6H_3), 7.32 (d, $^4J_{H,H}$ = 2.2 Hz, 1H, arom. C_6H_3), 7.50 (d, $^4J_{H,H}$ = 2.5 Hz, 1H, arom. C_6H_2), 8.67 (s, 1H, CH=N, with satellite splitting on tin nuclei, $^3J_{H,Sn}$ = 50.9 Hz). ^{13}C NMR (100 MHz; $CDCl_3$; δ, ppm): 9.53, 13.82 ($J_{C,Sn}$ = 1046 Hz), 29.37, 31.27, 31.66, 34.05, 34.30, 35.24, 110.94, 117.04, 117.53, 126.76, 128.94, 130.86, 131.79, 138.23, 139.08, 140.90, 157.04, 161.95, 167.51.

Found, *m/z*: 558.2382 $[M + H]^+$. For $C_{29}H_{44}NO_2Sn$ calculated, *m/z*: 558.2394.

$(L^2)SnEt_2$ (V). The yield of a red powder was 0.090 g (49%).

IR (KBr; ν, cm^{-1}): 2994, 2927, 2906, 2867, 1611, 1589, 1558, 1531, 1477, 1461, 1444, 1430, 1420, 1384, 1361, 1323, 1303, 1280, 1254, 1233, 1200.

^1H NMR (400 MHz; $CDCl_3$; δ, ppm): 1.28 (t, $^3J_{H,H}$ = 7.8 Hz, 6H, Me), 1.33 (s, 9H, *t*-Bu), 1.35 (s, 9H, *t*-Bu), 1.34–1.38 (m, 4H, CH_2), 1.41 (s, 9H, *t*-Bu), 1.43 (s, 9H, *t*-Bu), 7.04 (d, $^4J_{H,H}$ = 2.5 Hz, 1H, arom. C_6H_2), 7.20 (d, $^4J_{H,H}$ = 2.1 Hz, 1H, arom. C_6H_2), 7.23 (d, $^4J_{H,H}$ = 2.1 Hz, 1H, arom. C_6H_2), 7.47 (d, $^4J_{H,H}$ = 2.5 Hz, 1H, arom. C_6H_2), 8.62 (s, 1H, CH=N, with satellite splitting on tin nuclei, $^3J_{H,Sn}$ = 50.9 Hz). ^{13}C NMR (100 MHz; $CDCl_3$; δ, ppm): 9.55, 13.20 ($J_{C,Sn}$ = 1200 Hz), 29.17, 29.38, 31.30, 31.73, 34.04, 34.48, 35.22, 35.24, 108.74, 117.25, 123.53, 128.82, 130.78, 131.21, 137.23, 138.00, 140.81, 156.06, 161.74, 167.02.

Found, *m/z*: 614.2995 $[M + H]^+$. For $C_{33}H_{52}NO_2Sn$ calculated, *m/z*: 614.3021.

$(L^3)SnEt_2$ (VI). The yield of a yellow finely crystalline powder was 0.088 g (50%).

IR (KBr; ν, cm^{-1}): 3111, 3078, 2957, 2906, 2870, 1608, 1585, 1556, 1532, 1521, 1477, 1407, 1386, 1360, 1341, 1314, 1252, 1196.

^1H NMR (400 MHz; $CDCl_3$; δ, ppm): 1.27 (t, $^3J_{H,H}$ = 7.9 Hz, 6H, Me), 1.31 (s, 9 H, *t*-Bu), 1.40 (s, 9 H, *t*-Bu), 1.53 (q, $^3J_{H,H}$ = 7.9 Hz, 4H, CH_2), 7.05 (d, $^4J_{H,H}$ = 2.5 Hz, 1H, arom. C_6H_2), 7.45 (d, $^4J_{H,H}$ = 2.5 Hz, 1H, arom. C_6H_2), 7.59 (d, $^4J_{H,H}$ = 2.5 Hz, 1H, arom. C_6H_2), 7.88 (d, $^4J_{H,H}$ = 2.5 Hz, 1H, arom. C_6H_2), 8.62 (s, 1H, CH=N, with satellite splitting on tin nuclei, ^3J(H,Sn) = 44.0 Hz). ^{13}C NMR (100 MHz; $CDCl_3$; δ, ppm): 9.37, 14.81, 29.32, 31.05, 34.09, 35.27, 116.89, 118.60, 119.47, 124.31, 129.50, 134.29, 137.01, 137.97, 139.46, 141.54, 154.39, 164.80, 169.17.

Found, *m/z*: 603.1020 $[M + Na]^+$. For $C_{25}H_{33}ClN_2NaO_4Sn$ calculated, *m/z:* 603.1041.

$(L^4)SnEt_2$ (VII). The yield of an orange finely crystalline powder was 0.125 g (72%).

IR (KBr; ν, cm^{-1}): 2954, 2907, 2865, 1612, 1591, 1572, 1552, 1528, 1449, 1425, 1400, 1385, 1330, 1300, 1253, 1231, 1200.

^1H NMR (400 MHz; $CDCl_3$; δ, ppm): 1.25 (t, $^3J_{H,H}$ = 7.9 Hz, 6H, Me), 1.31 (s, 9H, *t*-Bu), 1.40 (s, 9H, *t*-Bu), 1.44–1.56 (m, 4H, CH_2), 2.45 (m, 1H, CH_3), 7.02 (d, $^4J_{H,H}$ = 2.5 Hz, 1H, arom. C_6H_2), 7.28 (s, 1H, arom. C_6H_1), 7.53 (d, $^4J_{H,H}$ = 2.5 Hz, 1H, arom. C_6H_2), 8.61 (s, 1H, CH=N, with satellite splitting on tin nuclei, $^3J_{H,Sn}$ = 47.5 Hz). ^{13}C NMR (100 MHz; $CDCl_3$; δ, ppm): 9.39, 14.77, 17.91, 29.34, 31.14, 34.03, 35.24, 113.05, 116.82, 120.83, 123.76,

Table 1. Crystallographic data and experimental and structure refinement parameters for complexes **I**, **II**, **III**·CH_3CN, **VI**, and **VII**

Complex	Value				
	I	**II**	**III**·CH_3CN	**VI**	**VII**
Composition	$C_{37}H_{43}NO_2Sn$	$C_{41}H_{51}NO_2Sn$	$C_{35}H_{36}N_3O_4ClSn$	$C_{25}H_{33}N_2O_4ClSn$	$C_{26}H_{35}NO_2Cl_2Sn$
FW	652.41	708.51	716.81	579.67	583.14
T, K	100(2)	150(2)	150(2)	150(2)	150(2)
Crystal system	Monoclinic	Monoclinic	Triclinic	Monoclinic	Monoclinic
Space group	$P2_1/n$	$P2_1/n$	$P\bar{1}$	$P2_1/c$	$P2_1/c$
a, Å	9.4381(8)	11.6941(3)	9.2396(5)	19.7443(10)	17.1880(15)
b, Å	12.5194(11)	9.8529(3)	11.9088(9)	11.8612(6)	18.4035(15)
c, Å	27.030(2)	31.6663(9)	16.0028(9)	11.4313(6)	8.4091(7)
α, deg	90	90	98.764(2)	90	90
β, deg	91.237(3)	95.9380(10)	105.343(2)	104.086(2)	99.056(3)
γ, deg	90	90	98.459(2)	90	90
V, Å^3	3193.1(5)	3629.04(18)	1645.48(18)	2596.6(2)	2626.8(4)
Z	4	4	2	4	4
ρ_{calc}, mg/m^3	1.357	1.297	1.447	1.483	1.475
μ, mm^{-1}	0.833	0.738	0.900	1.119	1.199
Scan range over θ, deg	1.627–26.000	2.166–26.000	2.325–25.999	2.515–25.998	2.400–28.999
Number of measured/ independent reflections	18912/6263	27029/7122	14814/6430	22697/5107	25147/6982
Number of reflections with $I > 2\sigma(I)$	4848	6115	5740	3883	5432
R_{int}	0.0809	0.0337	0.0349	0.0618	0.0745
GOOF (F^2)	1.255	1.110	1.047	1.024	1.112
R_1/wR_2 ($I > 2\sigma(I)$)	0.0991/0.1742	0.0331/0.0708	0.0352/0.0700	0.0357/0.0676	0.0615/0.1221
R_1/wR_2 (for all parameters)	0.1271/0.1830	0.0424/0.0737	0.0416/0.0732	0.0570/0.0735	0.0837/0.1304
$\Delta\rho_{max}/\Delta\rho_{min}$, e Å^{-3}	1.328 /–4.321	0.597/–0.703	1.071/–1.070	0.672/–0.750	1.817/–1.696

129.17, 130.67, 132.89, 134.32, 138.70, 141.10, 154.59, 162.99, 168.19.

Found, *m/z*: 584.1104 $[M + H]^+$. For $C_{26}H_{36}Cl_2NO_2Sn$ calculated, *m/z*: 584.1132.

XRD of single crystals of the studied compounds was carried out on a Bruker D8 Venture automated diffractometer equipped with a CCD detector (graphite monochromator, λMoK_a = 0.71073 Å, ω and φ scan modes) at *T* = 150 K. An absorption correction was applied semiempirically using the SADABS program [37]. The structures were solved by a direct method using the SHELXT 2014/4 program [38] and refined first in the isotropic approximation and then in the anisotropic approximation using the SHELXL-2018/3 program [38] and OLEX2 [39]. Hydrogen atoms were placed in geometrically calculated positions and included in refinement by the riding model. The crystallographic parameters and structure refinement details are given in Table 1.

The structural data were deposited with the Cambridge Crystallographic Data Centre (CIF files CCDC nos. 2181140 (**I**), 2181142 (**II**), 2181143 (**III**·CH_3CN), 2181141 (**VI**), and 2181139 (**VII**)) and are available at deposit@ccdc.cam.ac.uk or http://www.ccdc.cam.ac.uk/data_request/cif.

RESULTS AND DISCUSSION

The starting redox-active Schiff bases L^1H_2–L^4H_2 acting as ligands were synthesized by the condensation of sterically hindered salicylaldehyde with *o*-aminophenols bearing different donor or acceptor substituents (Scheme 1).

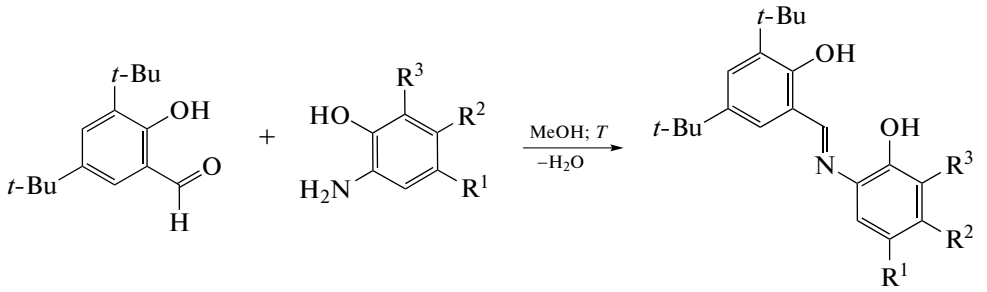

L^1H_2: R^1 = *t*-Bu; $R^2 = R^3 = H$ (55%)
L^2H_2: $R^1 = R^3$ = *t*-Bu; R^2 = H (62%)
L^3H_2: R^1 = Cl; R^2 = H; $R^3 = NO_2$ (62%)
L^4H_2: $R^1 = R^3$ = Cl; R^2 = Me (70%)

Scheme 1.

The yield of L^1H_2–L^4H_2 ranged from 55 to 70%. The structures of the compounds were confirmed by the ^1H and ^{13}C NMR, IR spectroscopy, and mass spectrometry data.

Tin complexes $LSnR_2$ (**I**–**VII**) were synthesized by the exchange reaction between the Schiff base and tin(IV) salt in a ratio of 1 : 1 in acetonitrile in the presence of triethylamine as the deprotonating agent (Scheme 2).

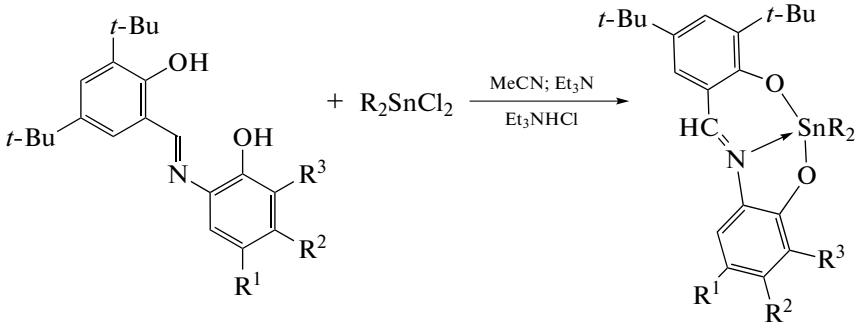

(**I**) L^1SnPh_2 (48%)
(**II**) L^2SnPh_2 (56%)
(**III**) L^3SnPh_2 (50%)
(**IV**) L^1SnEt_2 (60%)
(**V**) L^2SnEt_2 (49%)
(**VI**) L^3SnEt_2 (50%)
(**VII**) L^4SnEt_2 (72%)

Scheme 2.

The reactions were carried out under anaerobic conditions to avoid side processes of ligand oxidation. Complexes **I**–**VII** were isolated during filtration in air as red-orange crystalline powders in the yield up to 72%. The synthesized compounds are resistant to air oxygen and moisture. The compositions and structures of compounds **I**–**VII** were determined by ^1H and ^{13}C NMR, IR spectroscopy, and high resolution mass spectrometry. The IR spectra of the synthesized compounds are characterized by a set of vibration bands of the ligands composing the complexes. For instance, the IR spectra of complexes **I**–**VII** exhibit intense stretching vibration bands of the ordinary C–O bonds of the phenolate ligands (1200–1250 cm^{-1}), and intense bands corresponding to stretching vibrations of the C=N bond are observed in a range of 1586–1612 cm^{-1}. An insignificant shift of the stretching vibration bands of the C=N bond (1615–1620 cm^{-1}) compared to those of free ligands indicates the coordination of the imine nitrogen atom to the metal center [40]. The ^1H and ^{13}C NMR spectra contain signals from protons (and, correspondingly, carbon atoms) of all groups and fragments of these complexes (see Experimental). For example, a singlet from the imine CH=N group is observed in a range of 8.61–8.72 ppm with satellite splitting on tin nuclei with $^3J_{H,Sn} = 44.0$–62.5 Hz, which confirms the coordination of the imine group to the tin atom in a solution.

The crystals of complexes **I**–**III**, **VI**, and **VII** suitable for XRD were grown from solutions in acetonitrile. The crystals of complex **III** contain solvated acetonitrile molecules in a ratio of 1 : 1. Selected bond lengths and bond angles are listed in Table 2. The molecular structures of complexes **I**–**VI** are shown in Figs. 1–4, respectively.

In complexes **I**–**VI** (Figs. 1–4), the coordination number of the central tin atom is five. The τ parameter describing the deviation of the coordination polyhedron of the metal in the pentacoordinate complexes from ideal tetragonal ($\tau = 0$) and trigonal ($\tau = 1$) bipyr-

Table 2. Selected bond lengths (Å) and bond angles (deg) in complexes **I**, **II**, **III**·CH_3CN, **VI**, and **VII**

Bond	*d*, Å				
	I	**II**	**III**·CH_3CN	**VI**	**VII***
Sn(1)–O(1)	2.079(6)	2.0672(17)	2.108(2)	2.143(2)	2.191(3)
Sn(1)–O(2)	2.081(6)	2.0577(18)	2.083(2)	2.101(2)	2.152(3)
Sn(1)–N(1)	2.179(7)	2.215(2)	2.165(2)	2.168(3)	2.207(4)
Sn(1)–C(14)	2.132(8)	2.125(3)	2.127(3)	2.116(3)	2.127(5)
Sn(1)–C(16)				2.118(4)	2.125(4)
Sn(1)–C(20)	2.115(9)	2.125(3)	2.109(3)		
O(1)–C(1)	1.325(11)	1.337(3)	1.312(3)	1.315(4)	1.326(5)
O(2)–C(8)	1.324(10)	1.323(3)	1.323(3)	1.313(4)	1.304(5)
N(1)–C(2)	1.432(11)	1.429(3)	1.425(4)	1.427(4)	1.416(6)
N(1)–C(7)	1.287(11)	1.288(3)	1.305(4)	1.312(4)	1.313(5)
			ω, deg		
O(1)Sn(1)O(2)	157.4(3)	151.48(8)	160.66(7)	155.09(9)	155.50(12)
O(1)Sn(1)N(1)	77.2(3)	75.63(8)	76.75(8)	75.29(10)	74.94(12)
O(2)Sn(1)N(1)	83.2(3)	83.13(8)	84.51(8)	80.87(10)	80.80(13)
C(14)Sn(1)C(20)	123.3(4)	122.44(10)	121.22(11)		
C(14)Sn(1)C(16)				130.96(15)	152.50(19)
N(1)Sn(1)C(14)	130.6(3)	136.69(9)	113.13(9)	120.05(14)	100.23(16)
N(1)Sn(1)C(20)	105.9(3)	100.79(9)	125.35(10)		
N(1)Sn(1)C(16)				08.90(12)	106.99(16)

* Sn(1)–O(1)' 2.794(3) Å; O(1)Sn(1)O(1)' 71.67(12)°; O(2)Sn(1)O(1), 132.83(12)°.

amid [41] is 0.44 (**I**), 0.25 (**II**), 0.59 (**III**), and 0.58 (**VI**). Thus, the coordination environment of tin in complexes **I** and **II** is described best of all as a strongly distorted tetragonal pyramidal one (the O(1), O(2), N(1), and C(14) atoms lie in the pyramid base), and that in complexes **III** and **VI** is described as a distorted trigonal bipyramidal environment (the base is formed by the N(1), C(14), and C(20) atoms (in **III**) or C(16) (in **VI**)). Similar distortions of coordination polyhedra have previously been described for resem-

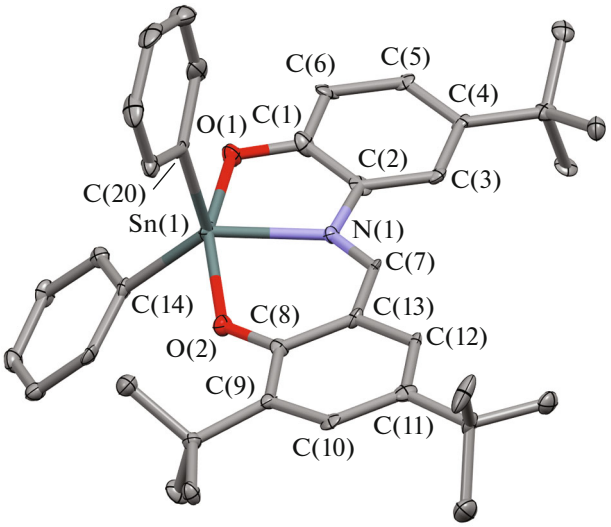

Fig. 1. Molecular structure of complex **I** according to the XRD data. Hydrogen atoms are omitted.

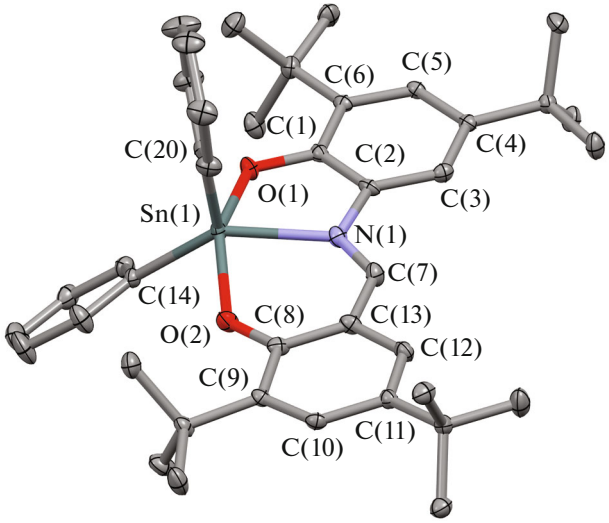

Fig. 2. Molecular structure of complex **II** according to the XRD data. Hydrogen atoms are omitted.

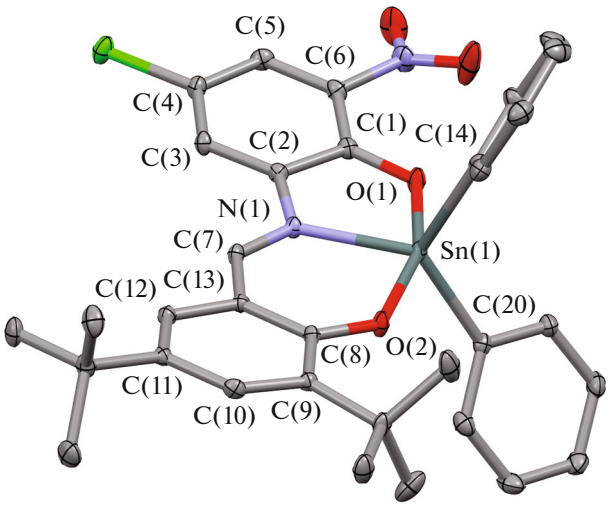

Fig. 3. Molecular structure of complex **III** according to the XRD data. Hydrogen atoms are omitted.

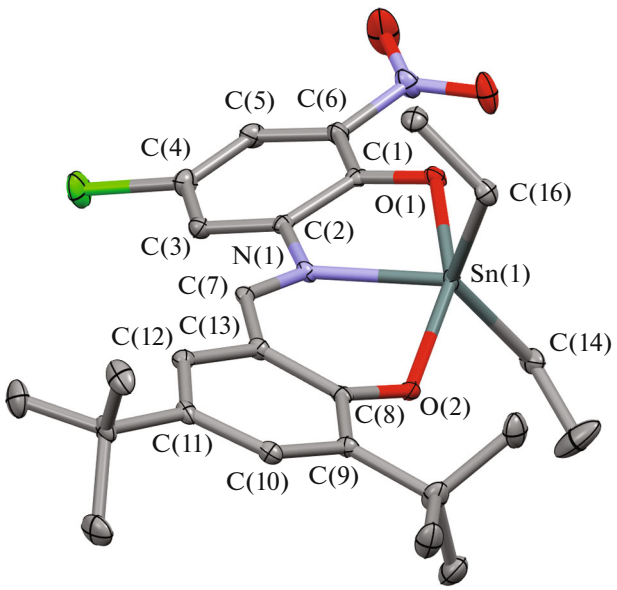

Fig. 4. Molecular structure of complex **VI** according to the XRD data. Hydrogen atoms are omitted.

bling pentacoordinate complexes of dimethyl-, dibutyl-, and diphenyltin(IV) with the tridentate O,N,O' ligands [20, 42–44]. Interestingly, the degree of deviation of the chelate cycles from the plane in the complexes and the degree of distortion of the O,N,O' ligands are different, which is confirmed by different torsion angles and shifts of the central tin atom from the plane of the chelating fragments of the ligand (Fig. 5, Table 3).

On the one hand, the Sn(1)–O(1) and Sn(1)–O(2) distances (2.079(6) and 2.081(6) Å in **I**, 2.0577(18) and 2.0672(17) Å in **II**, 2.083(2) and 2.108(2) Å in **III**, 2.101(2) and 2.143(2) Å in **VI**) correspond to the sum of covalent radii of tin and oxygen (2.1 Å: r_{cov} (Sn) = 1.36 Å, r_{cov}(O) = 0.73 Å [45]). On the other hand, the Sn–N distances (2.165(2)–2.215(2) Å) insignificantly exceed the sum of covalent radii of tin and nitrogen (r_{cov}(Sn) = 1.36 Å, r_{cov}(N) = 0.74 Å [45]). Similar bond lengths lie in the ranges characteristic of the related tin(IV) complexes with chelating O,O and O,N ligands [5, 7, 33, 46, 47].

In all structurally studied complexes, the C–O bond lengths range from 1.31 to 1.33 Å, which corresponds to the ordinary carbon–oxygen bonds in analogous ligands and confirms their dianionic structures [5, 7, 29, 33, 46, 47]. The six-membered carbon rings C(16) and C(8–13) are aromatic with average bond lengths of 1.393 and 1.405 Å in complex **I**, 1.398 and 1.401 Å in complex **II**, 1.395 and 1.404 Å in complex **III**, 1.398 and 1.404 Å in complex **VI**, and 1.396 and 1.408 Å in complex **VII**. The C(7)–N(1) bonds (1.287–1.312 Å) are shortened and correspond to conjugated imine bonds [14, 48–51]. Thus, the O,N,O' ligand in the complexes is dianionic iminobis(phenolate). In complexes **I**, **II**, **III**, and **VI**, this O,N,O' ligand is bound by the central tin atom via the tridentate mode. The situation is different for complex **VII**. This complex in the crystalline state forms dimers due to pairwise bridging coupling between the O(1) oxygen

Table 3. Selected structural characteristics of complexes **I**–**III**, **VI**, and **VII**

Complex	Angle between planes Sn(1)O(2)N(1) and O(2)C(8–13)C(7)N(1), deg	Torsion angles O(2)C(8)C(7)N(1)/ O(2)C(8)C(13)C(7), deg	Distance "plane O(1)C(1–6)N(1) ...Sn(1)," Å	Distance "plane O(2)C(8–13)C(7)N(1)...Sn(1)", Å	Torsion angle O(1)C(1)C(2)N(1), deg	Inflection angle of chelate cycle over O(1)...N(1) line, deg
I	19.92	1.35/–3.18	0.07	0.55	–2.63	<1
II	18.75	5.16/–0.52	0.304	0.534	–0.02	10.27
III	7.10	4.76/–2.86	0.23	0.216	4.90	7.23
VI	30.30	–7.89/–1.27	0.52	0.81	–3.56	16.32
VII	12.22	5.06/9.90	0.576	0.325	3.08	17.74

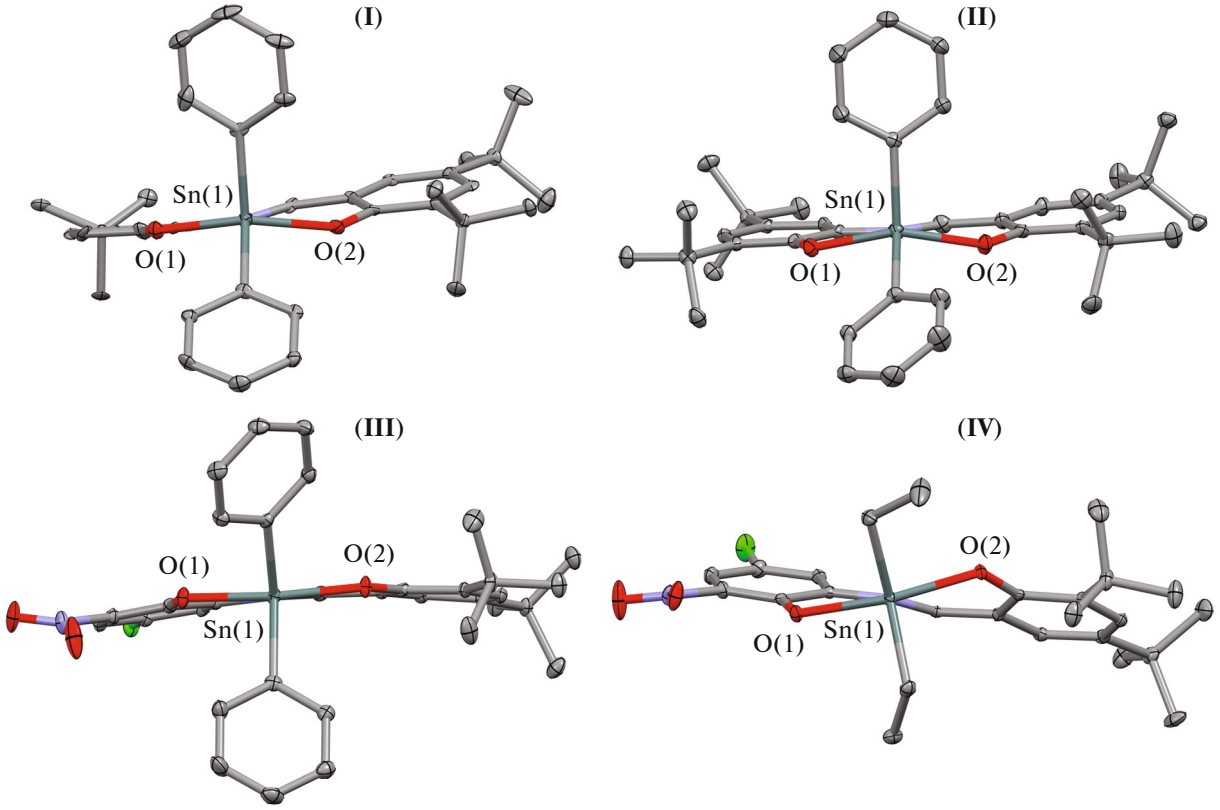

Fig. 5. View of molecules of complexes **I**, **II**, **III**, and **VI** along Sn–N bond.

and Sn(1) tin atoms of the mononuclear complexes (Fig. 6). The Sn(1)–O(1)' distances are 2.794(3) Å, which is somewhat longer than those in the related dimeric tin complexes with bridging alkyloxy groups (2.38–2.44 Å [52, 53]) but corresponds to the range of these bonds in the dimeric diorganyltin(IV) complexes with bridging phenolate groups (2.7–3.1 Å, [43, 52, 53]). Owing to these interactions, the coordination sphere of the tin atoms is built up to a strongly distorted octahedral geometry in which ethyl groups occupy axial positions.

The electrochemical properties of free ligands L^1H_2–L^4H_2 were initially studied by cyclic voltammetry (CV) to understand processes occurring during redox transformations of the tin(IV) complexes (Table 4). The electrooxidation of the free Schiff bases in dichloromethane proceeds in two steps (Fig. 7). The first irreversible peak is observed in a potential range of 1.20–1.23 V for L^1H_2, L^2H_2, and L^4H_2.

As found previously, the compounds of a similar type are characterized by intramolecular cyclization reactions that occur under electrochemical conditions with the formation of the corresponding benzoxazoles [54–56]. Depending on the solvent and electrode material used, this process can proceed as one two-electron or two consecutive one-electron steps. One irreversible peak is detected in dichloromethane in the indicated potential range, which assumes the two-electron process (Scheme 3).

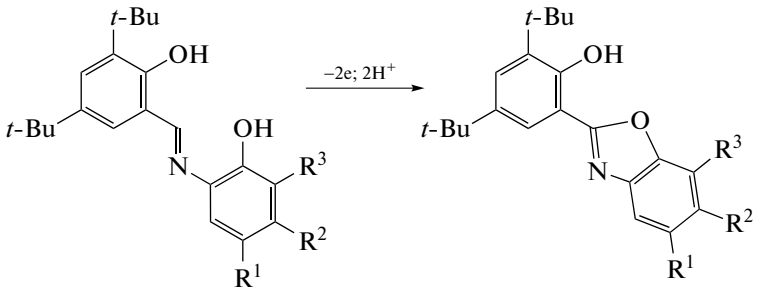

Scheme 3.

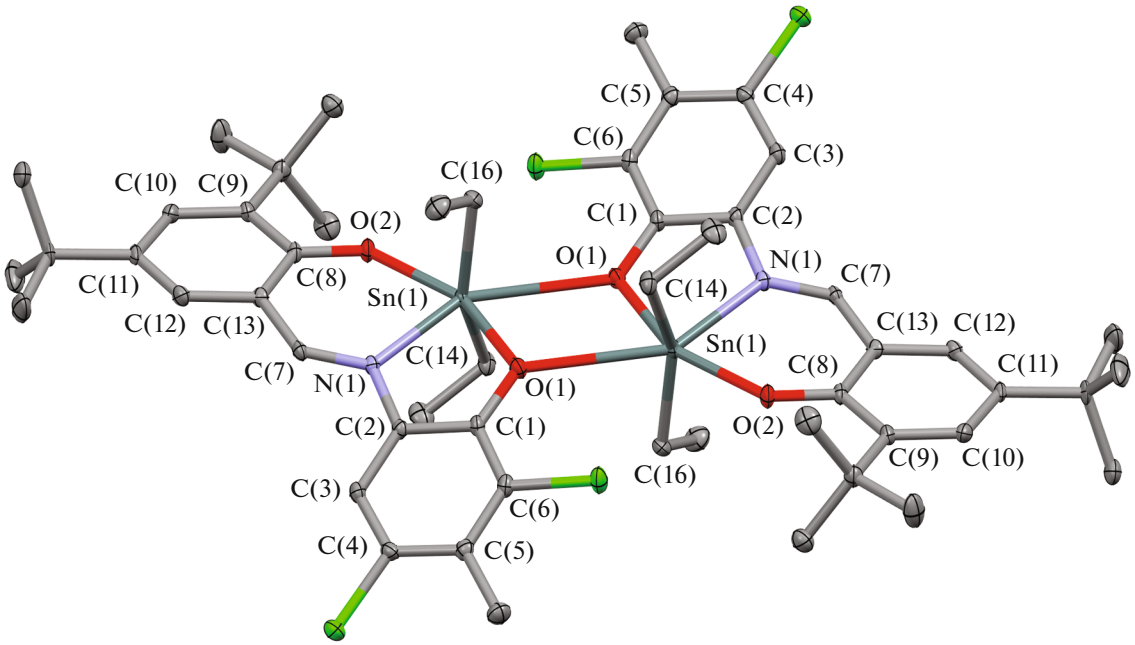

Fig. 6. Molecular structure of dimer **VII** in crystal according to the XRD data. Ellipsoids of 30% probability. Hydrogen atoms are omitted.

The microelectrolysis of L^1H_2 (1.15 V) was carried out to confirm the reaction mechanism. The calculated number of electrons involved in the electrode processes was 2, which confirms that the above indicated transformations occur. The replacement of the solvent by acetonitrile made it possible to observe the separation of one two-electron step into two one-electron processes in the case of compounds L^1H_2 and L^2H_2, and the second process is quasi-reversible and one-electron (Fig. 8).

This fact indicates a possibility of formation of the corresponding cyclic radical (Scheme 4), which has previously been detected for ferrocenyl-substituted iminophenols [2].

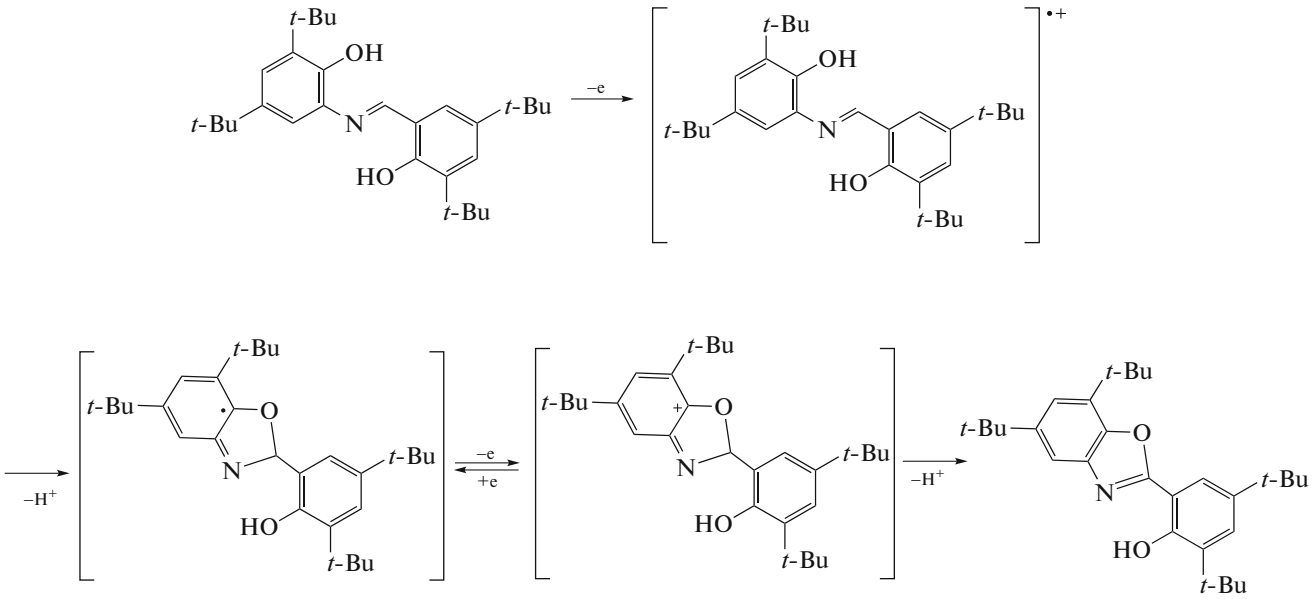

Scheme 4.

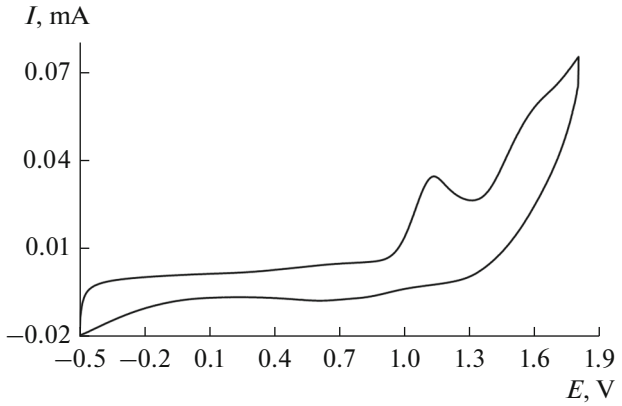

Fig. 7. Cyclic voltammogram for the oxidation of L^1H_2 in the potential sweep range from −0.5 to 1.8 V (CH_2Cl_2, GC anode, Ag/AgCl/KCl, 0.1 M n-Bu_4ClO_4, $c = 3 \times 10^{-3}$ mol/L, argon).

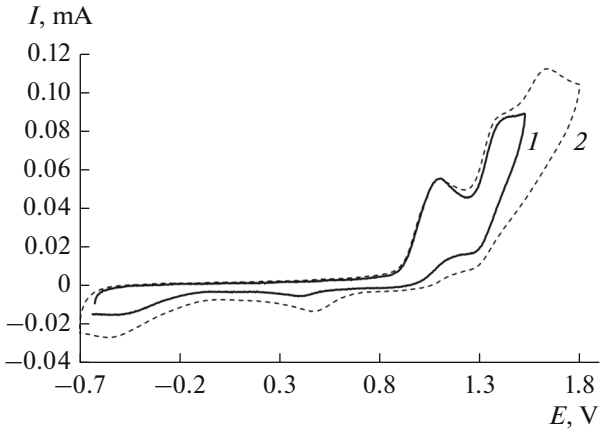

Fig. 8. Cyclic voltammograms for the oxidation of L^2H_2 at the potential sweep rate (*1*) from −0.6 to 1.5 V and (*2*) from −0.7 to 1.8 V (CH_3CN, GC anode, Ag/AgCl/KCl, 0.1 M n-Bu_4ClO_4, $c = 3 \times 10^{-3}$ mol/L, argon).

The presence of *tert*-butyl groups favors the stabilization of similar intermediates, since the current ratio increases to 0.9 compared to the data for L^1H_2. The third anodic peak corresponds to the oxidation of the phenol group. The number of electrons involved in the reaction is 2. The electrolysis at the controlled potential (1.20 V) for compound L^2H_2 results in the formation of the cyclization product characterized by two anodic peaks (1.45 and 1.70 V). An analysis of the reaction products using IR spectroscopy showed that the C=N stretching vibration bands (1584, 1615 cm^{-1}) detected in the spectrum of the starting Schiff base disappear after electrolysis, and a new intense band appears at 1554 cm^{-1}, which is more characteristic of benzoxazoles.

In the case of L^1H_2 and L^2H_2, the introduction of the donor hydroxy and *tert*-butyl groups leads to the shift of the oxidation potentials to the cathodic range compared to the earlier studied iminophenol (1.27 V) [54]. The oxidation of Schiff base L^3H_2 is observed at the potentials shifted to the anodic range, which is due to the influence of the electron-withdrawing nitro group. Unlike the above considered compounds, the first anodic peak for L^3H_2 is quasi-reversible and the number of transferred electrons exceeds unity. The decrease in the current ratio to 0.5 indicates that the fast chemical step of deprotonation occurs. In this case, the presence of the electron-withdrawing nitro group and the chlorine atom deactivating the aromatic ring results in the formation of a poorly stable dication subjected to deprotonation and subsequent cyclization. The peak observed at 1.50–1.56 (CH_2Cl_2) or 1.66 V (MeCN) can be assigned to the oxidation of the phenolic hydroxyl in the formed benzoxazole.

The irreversible peak characteristic of azomethine linker reduction is detected in the potential range from −1.58 to −1.75 V for the studied Schiff bases L^1H_2, L^2H_2, and L^4H_2 [57]. For L^3H_2, the cathodic step is detected at the potential shifted to the anodic range

Table 4. Redox potentials of Schiff bases L^1H_2–L^4H_2 obtained by the CV method*

Compound	Solvent	E_p^{ox1}, V	I_c/I_a	E_p^{ox2}, V	I_c/I_a	E_p^{ox3}, V	E_p^{red1}, V	E_p^{red2}, V
L^1H_2	CH_2Cl_2	1.22		1.56			−1.75	
	CH_3CN	1.02		1.38**	0.50	1.66	−1.73	
L^2H_2	CH_2Cl_2	1.23		1.56				
	CH_3CN	1.05		1.33**	0.90	1.66		
L^3H_2	CH_2Cl_2	1.30**	0.50	1.83			−0.69	−1.55
	CH_3CN	1.21**	0.50	1.55		1.66	−0.67	−1.51
L^4H_2	CH_2Cl_2	1.22		1.51			−1.60	
	CH_3CN	1.21		1.48			−1.58	

* GC electrode, 0.1 M n-Bu_4ClO_4, $c(LH_2) = 3 \times 10^{-3}$ mol/L, Ar, versus Ag/AgCl/KCl (sat.).
** The half-wave potential for the quasi-reversible process.

Table 5. Redox potentials of complexes **I**–**VII** obtained by the CV method*

Compound	$E_{1/2}^{ox1}$, V	I_c/I_a	$E_{1/2}^{ox2}$, V	I_c/I_a	E_p^{ox3}, V	$E_{1/2}^{red1}$, V	I_a/I_c	$E_{1/2}^{red2}$, V	ΔE_{el}, eV
$(L^1)SnPh_2$ (**I**)	1.16	0.94	1.45	0.50	1.69	−1.44	0.82		2.60
$(L^2)SnPh_2$ (**II**)	1.07	1.00	1.55**			−1.49	0.78		2.56
$(L^3)SnPh_2$ (**III**)	1.59**					−1.05**		−1.25	2.64
$(L^1)SnEt_2$ (**IV**)	1.03	0.45	1.33**		1.58	−1.58	0.80		2.61
$(L^2)SnEt_2$ (**V**)	0.96	1.00	1.32	0.45	1.61	−1.63	0.50		2.59
$(L^3)SnEt_2$ (**VI**)	1.34**		1.55	0.76	1.82	−1.09**		−1.73	2.43
$(L^4)SnEt_2$ (**VII**)	1.23**		1.40	0.70	1.74	−1.40	0.71		2.68
$L'Sn^tBu_2$ [20]	1.19**					−0.78**			1.97
$L''Sn^tBu_2$ [20]	0.92**		1.38**			−1.37**			2.29

* CH_2Cl_2, GC electrode, 0.1 M n-Bu_4ClO_4, $c = 3 \times 10^{-3}$ mol/L, Ar, versus Ag/AgCl/KCl (sat.).
** Peak potential.

(Table 4), which is associated with the participation of the redox-active nitro group in the electrode reaction. An additional quasi-reversible peak at −1.52 V corresponding to the deeper reduction of the free ligand is observed with an increase in the potential sweep range.

The electrochemical properties of the tin(IV) complexes were studied by the CV method (Table 5).

The electrochemical oxidation of complexes **I**, **II**, and **IV**–**VII** at the GC electrode in dichloromethane proceeds in two or three consecutive steps (Fig. 9).

Unlike the earlier studied tin(IV) complexes with the O,N,O-donor Schiff bases [20, 58, 59], for complexes **I**, **II**, **IV**, and **V** the first anodic peak is quasi-reversible and one-electron, indicating the formation of relatively stable (in the time scale of CV experiment) monocationic species (Fig. 10).

A specific feature of the used Schiff bases is the presence of bulky *tert*-butyl groups that efficiently stabilize the oxidized form of the ligand. According to the values of current ratios (Table 5) for the diphenyltin(IV) derivatives, it can be concluded that no significant effect on an increase in the stability of the generated monocation is observed on going from complex **I** to complex **II**. At the same time, the stabilization of the oxidized form for complex **V** is more pronounced in the pair of compounds **IV** and **V**. On the CV curves of complexes **I** and **V** (Fig. 11), the second quasi-reversible step characterizes the generation of the relatively stable dication.

The possibility of an efficient electron density delocalization in the structure of the redox-active ligand makes it possible to detect the doubly oxidized form of the ligand. In the case of complex **II**, the second redox transition has a two-electron level for the current, whereas one two-electron process is divided into two consecutive steps for compounds **I**, **IV**, and **V** (Scheme 5).

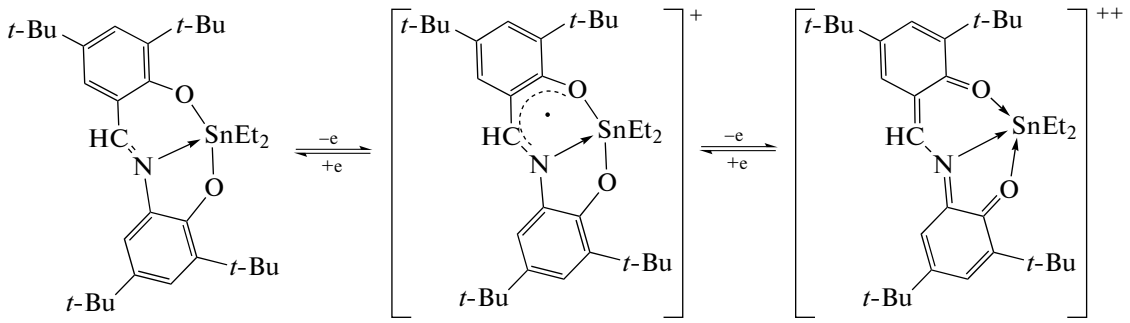

Scheme 5.

The dication formed upon the electrooxidation of complexes **I** and **V** has a lower stability (I_c/I_a), and the reverse branches of the voltammograms exhibit peaks of the decomposition products of the complex. The

third anodic step corresponds to a deeper oxidation of the ligand.

The first anodic step is irreversible for complexes **III**, **VI**, and **VII**. In the case of compound **III**, this is the multielectron process leading to the decomposition of the complex (Fig. 12).

The replacement of phenyl groups by ethyl groups at the tin atom in complex **VI** results in the detection of three redox transitions (Fig. 13). A similar electrochemical pattern is observed for compound **VII**.

A specific feature of the electrochemical behavior is the irreversibility of the first one-electron redox transition indicating the occurrence of the subsequent chemical step due to which an intermediate relatively stable within the CV experiment time is formed. The second redox process is characterized by a higher current ratio than that for complexes **I** and **II**. In this case, two parallel processes are possible: the intramolecular cyclization of the ligand in the coordination sphere of the metal or labile Sn–C bond cleavage and ethyl radical elimination, which was earlier observed for the tin(IV) and antimony(V) complexes with the redox-active ligands [60, 61]. An increase in the stability of the species generated at the second oxidation step can indirectly show a higher probability of intramolecular cyclization in the coordination sphere of the metal with the formation of the heterocyclic radical (Scheme 6).

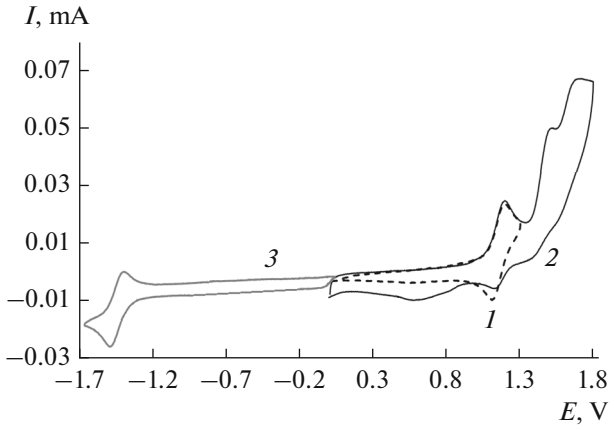

Fig. 9. Cyclic voltammograms for the oxidation–reduction of complex **I** at the potential sweep rate (*1*) from 0 to 1.30 V, (*2*) from 0 to 1.80 V, and (*3*) from 0 to −1.65 V (CH_2Cl_2, GC anode, Ag/AgCl/KCl, 0.1 M n-Bu_4ClO_4, $c = 3 \times 10^{-3}$ mol/L, argon).

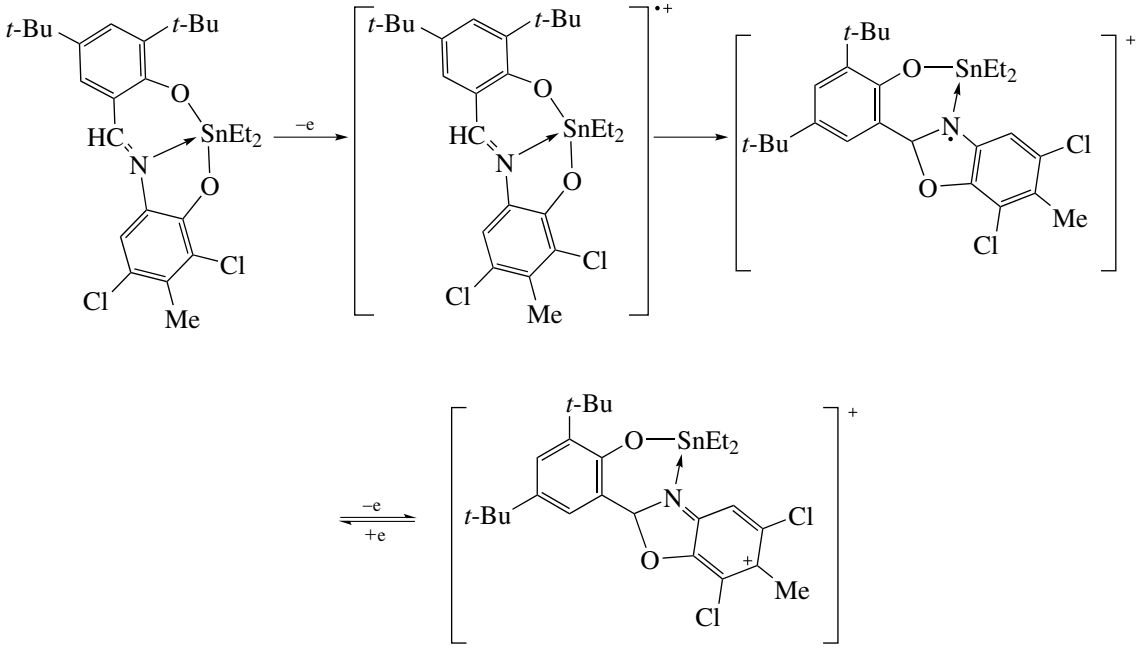

Scheme 6.

However, the current ratio for the second step is lower than unity, which assumes the occurrence of the subsequent chemical step: the deprotonation of the tertiary carbon atom with benzoxazole formation. The third anodic peak corresponds to the further deeper oxidation of the ligand. To confirm this scheme, we carried out the microelectrolysis of complex **VI** at a potential of 1.40 V (1.5 h). No evolution of gaseous products was observed upon to the reaction, which indirectly shows the absence of the Sn–C bond cleavage. The intensity of the first oxidation peak decreased during electrolysis at a constant value of the second anodic peak. The number of electrons involved in the electrode process was unity.

Common regularities are observed in the cathodic range for complexes **I**, **II**, **IV**, **V**, and **VII**: the CV curves

have one-electron quasi-reversible peak in the potential range from −1.40 to −1.63 V (Figs. 9, 10) corresponding to the formation of the relatively stable radical anion (Scheme 7).

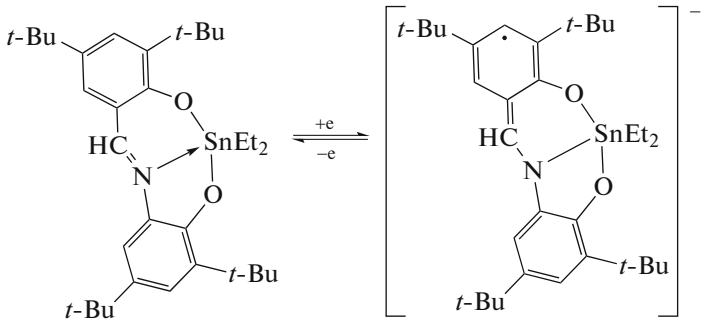

Scheme 7.

Unlike the free Schiff bases for which the reduction proceeds as a two-electron irreversible step, the coordination of the nitrogen atom of the imino group to the metal center favors the stabilization of the anion-radical form of the ligand. The organic substituents at the tin atom affect the reduction potentials. In the case of pairs of compounds **I** and **II**, as well as **III** and **IV** (Table 5), the replacement of the phenyl group by the ethyl group favors the shift of $E_{1/2}^{red1}$ to the cathodic range by 0.14 V. For complexes **V** and **VII**, the substitution of two *tert*-butyl groups in the ligand by chlorine atoms, on the contrary, results in the shift of the cathodic peaks to the anodic range by 0.18 V, which assumes, correspondingly, the facilitation of the reduction process. The detected values of $E_{1/2}^{red1}$ are well consistent with the earlier obtained data for the tin(IV) complexes (from −1.32 to −1.48 V) [7].

The mechanism of reduction of complexes **III** and **VI** becomes more complicated because of the electroactive NO_2 group. Their CV curves, as that for L^3H_2, exhibit an irreversible cathodic peak shifted to the cathodic range compared to that of the free ligand (Fig. 12). Taking into account the detected potential, we can assume that nitro groups is involved in the electrode process. In turn, the irreversibility of this step is related to a possibility of the intramolecular electron transfer and subsequent elimination of the chloride anion. The second cathodic peak (−1.25 V) for complex **III**, which is quasi-reversible and shifted according to the withdrawing influence of the substituents, can be assigned to the reduction of the azomethine linker. The potential of the third redox transition for complex **III** at −1.51 V coincides with that for free ligand L^3H_2 (Table 4), indicating the involvement of the reduced form of the NO_2 group in further transformations. For complex **VI**, the second cathodic peak has a multielectron nature and is characterized by the participation of both redox-active fragments.

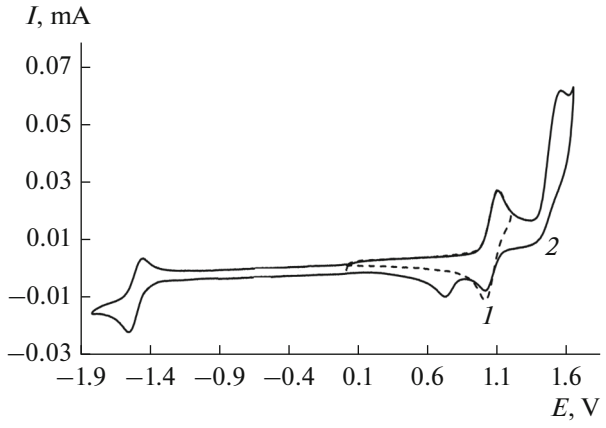

Fig. 10. Cyclic voltammograms for the oxidation–reduction of complex **II** at the potential sweep rate (*1*) from 0 to 1.20 V and (*2*) from −1.80 to 1.70 V (CH_2Cl_2, GC anode, Ag/AgCl/KCl, 0.1 M n-Bu_4ClO_4, $c = 3 \times 10^{-3}$ mol/L, argon).

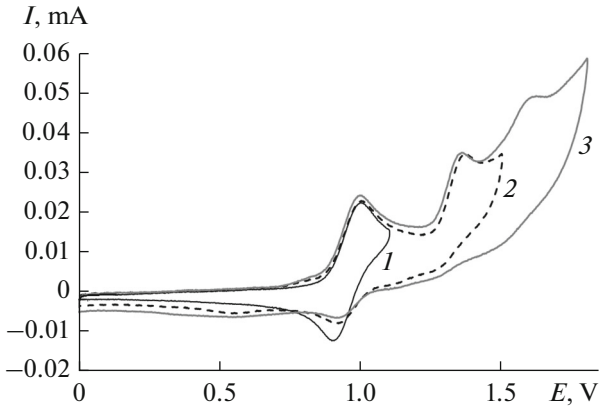

Fig. 11. Cyclic voltammograms for the oxidation of complex **V** at the potential sweep rate (*1*) from 0 to 1.15 V, (*2*) from 0 to 1.50 V, and (*3*) from 0 to 1.80 V (CH_2Cl_2, GC anode, Ag/AgCl/KCl, 0.1 M n-Bu_4ClO_4, $c = 3 \times 10^{-3}$ mol/L, argon).

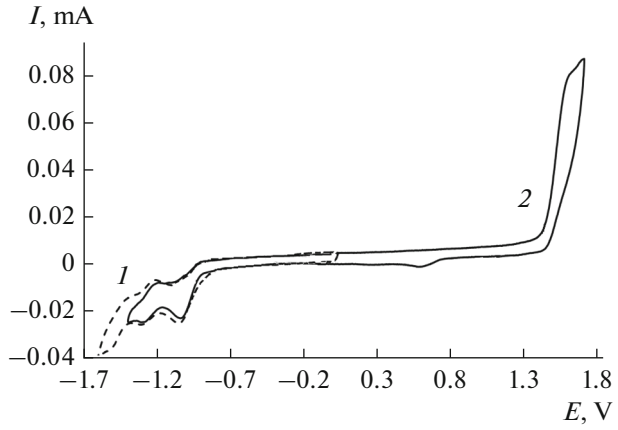

Fig. 12. Cyclic voltammograms for the oxidation–reduction of complex **III** at the potential sweep rate (*1*) from 0 to −1.60 V and (*2*) from −1.40 to 1.70 V (CH_2Cl_2, GC anode, Ag/AgCl/KCl, 0.1 M n-Bu_4ClO_4, $c = 3 \times 10^{-3}$ mol/L, argon).

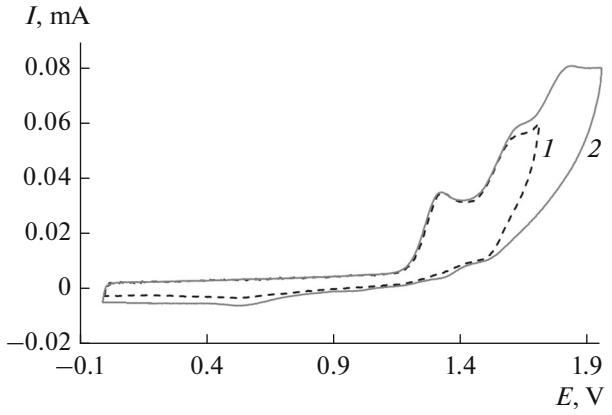

Fig. 13. Cyclic voltammograms for the oxidation of complex **VI** at the potential sweep rate (*1*) from 0 to 1.70 V and (*2*) from 0 to 1.95 V (CH_2Cl_2, GC anode, Ag/AgCl/KCl, 0.1 M n-Bu_4ClO_4, $c = 3 \times 10^{-3}$ mol/L, argon).

It has previously been found that the tin(IV) complexes with the O,N,O-donor Schiff bases acting as ligands absorb in the visible spectral range at 480–490 nm, which is closest to the maximum solar radiation [20]. This specific feature makes it possible to consider similar compounds as a basis for manufacturing electron-withdrawing materials involved in the work of photoelectrical devices. The energy gap (ΔE), being the difference between the energies of the frontier orbitals, is one of the main parameters used for the evaluation of a possibility of using substances in photoelectrical devices. This parameter predetermines the efficiency of solar radiation absorption and the color of the emitted light in optoelectronic devices [62].

The value of ΔE can theoretically be determined using quantum chemical calculations or can experimentally be measured using electrochemistry or UV-visible spectroscopy. Electrochemical methods are widely applied for the determination of the electrochemical gap ΔE_{el}, since the standard reduction and oxidation potentials correlate with the LUMO and LOMO energies. In the case of complexes **I**, **II**, **IV**, and **V**, this value was determined as the difference in half-wave potentials for the first redox processes, whereas the value is determined as the difference in peaks for compounds **III**, **VI**, and **VII**. The values of ΔE_{el} range from 2.43 to 2.68 eV (Table 5), and the minimum parameter was obtained for the $(L^3)SnEt_2$ complex. The calculated values exceed the results obtained for the related tin complexes (Table 5). In the most part of cases, the ΔE parameter determined from the electrochemical data can be overestimated compared to the spectral measurements for the polymers and crystalline materials [62]. We studied the activity of the complexes and ligands in the UV-visible spectral range (300–600 nm) in chloroform (Table 6).

The spectra of Schiff bases L^1H_2, L^2H_2, and L^4H_2 exhibit an absorption maximum at 378–382 nm caused by the intraligand π–π* transition characteristic of the enolimine form of compounds of this type [21]. The presence of the electron-withdrawing NO_2 group in L^3H_2 results in the bathochromic shift of this absorption band at 405 nm. Unlike the free Schiff bases, the spectra of the studied tin(IV) complexes exhibit two or three absorption bands in this spectral range with an intense maximum at 473–493 nm (Table 6, Fig. 14).

The interaction of the deprotonated form of the ligands with the organometallic tin(IV) derivatives leads to the bathochromic shift of the absorption maximum to the long-wavelength range, which is visually expressed as a change in the color of the solutions from pale yellow to bright red. The spectra of compounds **I**, **II**, **IV**, **V**, and **VII** are characterized by two absorption bands, the first of which is related to the intramolecular charge transfer in the ligand (π–π* and n–π*), and the second more intense band (473–493 nm) characterizes the metal-to-ligand charge transfer. The detected values of λ_{max} are well consistent with the known literature data for the related tin(IV) complexes [33, 63, 64]. For compounds **III** and **VI**, the presence of the chromophoric nitro group induces an additional intraligand n–π* charge transfer at 418 or 420 nm [22].

The influence of substituents in the redox-active ligand on the position of a maximum in a range of 463–493 nm should be noted. For complexes **IV**–**VII**, the replacement of *tert*-butyl substituents by chlorine atoms exerts almost no effect on the value of λ_{max}, whereas the introduction of the nitro group leads to the bathochromic shift to 493 nm. Similar regularities are characteristic of complexes **I**–**III**, but the effect is less pronounced. A similar behavior can be explained by the participation of the redox-active nitro group in the electron density redistribution in the conjugated

Table 6. Spectra data for complexes **I**–**VII** and ligands L^1H_2–L^4H_2 in $CHCl_3$ at 293 K

Compound	Absorption λ_{max}, nm (ε, 10^3 L mol^{-1} cm^{-1})	ΔE, eV
$(L^1)SnPh_2$ (**I**)	324 (8.26), 390 sh (5.42), 473 (14.80)	2.62
$(L^2)SnPh_2$ (**II**)	321 (18.80), 393 sh (5.81), 477 (16.51)	2.60
$(L^3)SnPh_2$ (**III**)	317 (8.52), 418 (8.82), 483 (17.24)	2.57
$(L^1)SnEt_2$ (**IV**)	316 (7.51), 390 sh (5.51), 476 (15.61)	2.61
$(L^2)SnEt_2$ (**V**)	328 (6.99), 394 sh (5.29), 481 (15.51)	2.58
$(L^3)SnEt_2$ (**VI**)	313 (7.95), 393 sh (5.66), 420 (7.93), 493 (17.58)	2.52
$(L^4)SnEt_2$ (**VII**)	328 (6.98), 394 sh (5.34), 482 (17.57)	2.57
L^1H_2	378 (6.82)	
L^2H_2	382 (8.45)	
L^3H_2	405 (6.91)	
L^4H_2	378 (9.68)	

system of the ligand. Organic groups at the tin(IV) atom also affect the shift of the absorption band, and the effect is more appreciable for the diethyl derivatives compared to the diphenyl-substituted tin complexes.

The energy gaps for the complexes were determined by the equation ΔE (eV) = $1240/\lambda_{max}$ and are observed in the narrow range from 2.52 to 2.62 eV. The values of ΔE are well consistent with ΔE_{el} obtained from the electrochemical results, which is characteristic of low-molecular-weight compounds for which the measurement inaccuracy for two different methods usually varies in a range of 5–7% [62]. The ΔE parameter is close to those of the previously studied tin complexes with the semiconductor properties [20], which provides possibilities for the design of new compounds and further study of their photophysical properties.

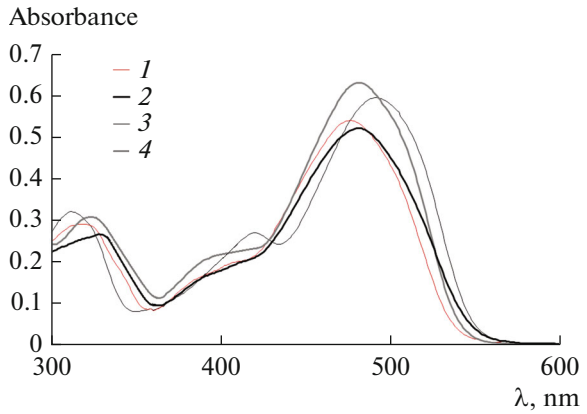

Fig. 14. Absorption spectra of complexes (*1*) **IV**, (*2*) **V**, (*3*) **VI**, and (*4*) **VII** in $CHCl_3$ at 293 K ($c = 3.5 \times 10^{-5}$ mol/L).

CONCLUSIONS

Thus, the redox-active O,N,O-donor Schiff bases were synthesized, and their electrochemical and spectral properties were studied. It was found that the electrooxidation of the ligands can result in intramolecular cyclization reactions. The reactions of the Schiff bases with R_2SnCl_2 afforded the series of the tin(IV) complexes. The molecular structures of complexes **I**–**IV** and **VII** were studied by XRD. Compounds **I** and **II** have a distorted tetragonal pyramidal coordination environment of the tin atom, whereas complexes **III** and **IV** are characterized by a distorted trigonal bipyramidal environment. Complex **VII** forms crystals in the form of dimers, and the coordination sphere of the metal is built up to a distorted octahedral geometry. In these compounds, the redox-active ligand exists in the dianionic iminobis(phenolate) form.

The formation of relatively stable (in the time scale of CV experiment) monocationic monoanionic complexes has first been detected for compounds **I**, **II**, **IV**, and **V** with *tert*-butyl groups in the redox-active ligand. For compounds **I** and **V**, a possibility of electron density delocalization in the ligand causes the stabilization of the doubly oxidized dicationic form of the ligand. The coordination of the nitrogen atom of the azomethine group favors the one-electron quasi-reversible process in the cathodic range and the formation of the corresponding monoanionic complexes in the case of compounds **I**, **II**, **IV**, **V**, and **VII**. The destabilization of the oxidized monocationic forms of complexes **III** and **VI** is observed in the presence of the electron-withdrawing nitro group in the ligand structure. As in the case of the free Schiff bases, an additional peak corresponding to the participation of the

NO_2 group in the redox process was detected in the cathodic range of the potential sweep.

An analysis of the potentials suggests that the complexes, on the one hand, are electron donors and are oxidized in the accessible potential range below 1.20 V and, on the other hand, act as weak electron acceptors. A similar dual behavior predetermines a possibility of their use for the initiation of photoinduced redox transformations or as electrocatalysts. The energy gaps between the frontier redox orbitals of the studied tin(IV) complexes calculated by two different methods (electrochemical and spectral) are characterized by fairly close values (2.43–2.68 eV). The position of the absorption band corresponding to the metal-to-ligand charge transfer was found to depend on both the nature of the substituents in the redox-active ligand and the structures of hydrocarbon groups at the tin atom.

FUNDING

This work was supported by the Russian Science Foundation, project no. 22-13-00118.

CONFLICT OF INTEREST

The authors declare that they have no conflicts of interest.

REFERENCES

1. Chen, W., Ou, W., Wang, L., et al., *Dalton Trans.*, 2013, vol. 42, p. 15678.
2. Smolyaninov, I.V., Poddel'sky, A.I., Baryshnikova, S.V., et al., *Appl. Organomet. Chem.*, 2018, vol. 32, p. e4121.
3. Smolyaninov, I.V., Burmistrova, D.A., Arsenyev, M.V., et al., *ChemistrySelect*, 2021, no. 6, p. 10609.
4. Dehghani-Firouzabadi, A.A., Sobhani, M., and Notash, B., *Polyhedron*, 2016, vol. 119, p. 49.
5. Bellan, E.V., Poddel'sky, A.I., Arsenyev, M.V., et al., *Eur. J. Inorg. Chem.*, 2016, vol. 33, p. 5230.
6. Berrones-Reyes, J.C., Munoz-Flores, B.M., Uscanga-Palomeque, A.C., et al., *ChemistrySelect*, 2020, vol. 5, p. 1623.
7. Baryshnikova, S.V., Poddel'sky, A.I., Bellan, E.V., et al., *Inorg. Chem.*, 2020, vol. 59, p. 6774.
8. Zoubi, W.A. and Ko, Y.G., *J. Organomet. Chem.*, 2016, vol. 822, p. 173.
9. Liu, X., Manzur, C., Novoa, N., et al., *Coord. Chem. Rev.*, 2018, vol. 357, p. 144.
10. Zhang, J., Xu, L., and Wong, W.-Y., *Coord. Chem. Rev.*, 2018, vol. 355, p. 180.
11. Berhanu, A.L., Gaurav, I., Mohiuddin, I., et al., *Trends Anal. Chem.*, 2019, vol. 116, p. 74.
12. Oiye, É.N., Ribeiro, M.F.M., Katayama, J.M.T., et al., *CRC Crit. Rev. Anal. Chem.*, 2019, vol. 49, p. 488.
13. Kaczmarek, M.T., Zabiszak, M., Nowak, M., et al., *Coord. Chem. Rev.*, 2018, vol. 370, p. 42.
14. More, M.S., Joshi, P.G., Mishra, Y.K., et al., *Mater. Today Chem.*, 2019, vol. 14, p. 100195.
15. Zoubi, W.A., Al-Hamdani, A.A.S., and Kaseem, M., *Appl. Organomet. Chem.*, 2016, vol. 30, p. 810.
16. Zafar, W., Sumrra, S.H., and Chohan, Z.H., *Eur. J. Med. Chem.*, 2021, vol. 222, p. 113602.
17. Ilyakina, E.V., Poddel'sky, A.I., Piskunov, A.V., et al., *Inorg. Chim. Acta*, 2013, vol. 394, p. 282.
18. Ilyakina, E.V., Poddel'sky, A.I., Fukin, G.K., et al., *Inorg. Chem.*, 2013, vol. 52, p. 5284.
19. Piskunov, A.V., Meshcheryakova, I.N., Piskunova, M.S., et al., *J. Mol. Struct.*, 2019, vol. 1195, p. 417.
20. Cantón-Díaz, A.M., Muñoz-Flores, B.M., Moggio, I., et al., *New J. Chem.*, 2018, vol. 42, p. 14586.
21. Zugazagoitia, J.S., Maya, M., Damian-Zea, C., et al., *J. Phys. Chem. A*, 2010, vol. 114, p. 704.
22. Lopez-Espejel, V., Gomez-Trevino, A., Munoz-Flores, B.M., et al., *J. Mater. Chem.*, 2021, vol. 9, p. 7698.
23. Khan, H.Y., Maurya, S.K., Siddique, H.R., et al., *ACS Omega*, 2020, vol. 5, p. 15218.
24. Khatkar, P. and Asija, S., *Phosphorus, Sulfur, Silicon Relat. Elem.*, 2017, vol. 192, p. 446.
25. Jiang, W., Qin, Q., Xiao, X., et al., *J. Inorg. Biochem.*, 2022, vol. 232, p. 111808.
26. Antonenko, T.A., Shpakovsky, D.B., Vorobyov, M.A., et al., *Appl. Organomet. Chem.*, 2018, vol. 32, p. e4381.
27. Galván-Hidalgo, J.M., Ramírez-Apan, T., Nieto-Camacho, A., et al., *J. Organomet. Chem.*, 2017, vol. 848, p. 332.
28. Nath, M. and Saini, P.K., *Dalton Trans.*, 2011, vol. 40, p. 7077.
29. Vinayak, R., Dey, D., Ghosh, D., et al., *Appl. Organomet. Chem.*, 2018, vol. 32, p. e4122.
30. Basu, S., Masharing, C., and Das, B., *Heteroat. Chem.*, 2012, vol. 23, p. 457.
31. Gonzalez, A., Gomez, E., Cortes-Lozada, A., et al., *Chem. Pharm. Bull.*, 2009, vol. 57, p. 5.
32. Basu, S., Gupta, G., Das, B., et al., *J. Organomet. Chem.*, 2010, vol. 695, p. 2098.
33. Tan, Y.-X., Zhang, Z.-J., Liu, Y., et al., *J. Mol. Struct.*, 2017, vol. 1149, p. 874.
34. Devi, J., Pachwania, S., Yadav, J., et al., *Phosphorus, Sulfur, Silicon Relat. Elem.*, 2020, vol. 196, p. 119.
35. Jimenez-Perez, V.M., Camacho-Camacho, C., Guizado-Rodriguez, M., et al., *J. Organomet. Chem.*, 2000, vols. 614–615, p. 283.
36. Gordon, A. and Ford, R., *The Chemist's Companion: A Handbook of Practical Data, Techniques, and References*, New York: Wiley, 1972.
37. Krause, L., Herbst-Irmer, R., Sheldrick, G.M., et al., *J. Appl. Crystallogr.*, 2015, vol. 48, p. 3.
38. Sheldrick, G.M., *Acta Crystallogr., Sect. A: Found. Adv.*, 2015, vol. 71, p. 3.
39. Dolomanov, O.V., Bourhis, L.J., Gildea, R.J., et al., *J. Appl. Crystallogr.*, 2009, vol. 42, p. 339.
40. Chans, G.M., Nieto-Camacho, A., Ramırez-Apan, T., et al., *Aust. J. Chem.*, 2015, vol. 69, no. 3, p. 279.
41. Addison, A.W., Rao, T.N., Reedijk, J., et al., *Dalton Trans.*, 1984, vol. 7, p. 1349.
42. González-Hernández, A. and Barba, V., *Inorg. Chim. Acta*, 2018, vol. 483, p. 284.

43. Zhang, Zh.-J., Zeng, H.-T., Liu, Y., et al., *Inorg. Nano-Met. Chem.*, 2018, vol. 48, p. 486.

44. Yenişehirli, G., Öztaş, N.A., Şahin, E., et al., *Heteroat. Chem.*, 2010, vol. 21, p. 373.

45. Batsanov, S.S., *Zh. Neorg. Khim.*, 1991, vol. 36, no. 12, p. 3015.

46. Galván-Hidalgo, J.M., Chans, G.M., Ramírez-Apan, T., et al., *Appl. Organomet. Chem.*, 2017, vol. 31, p. e3704.

47. García-López, M.C., Muñoz-Flores, B.M., Jiménez-Pérez, V.M., et al., *Dyes Pigm.*, 2014, vol. 106, p. 188.

48. Baryshnikova, S.V., Bellan, E.V., Poddel'sky, A.I., et al., *Inorg. Chem. Commun.*, 2016, vol. 69, p. 94.

49. Celebier, M., Sahin, E., Ancin, N., et al., *Appl. Organomet. Chem.*, 2007, vol. 21, p. 913.

50. Beltrán, H.I., Damian-Zea, C., Hernández-Ortega, S., et al., *J. Inorg. Biochem.*, 2007, vol. 101, p. 1070.

51. Pettinari, C., Marchetti, F., Pettinari, R., et al., *Inorg. Chim. Acta*, 2001, vol. 325, p. 103.

52. Baul, T.S.B., Addepalli, M.R., Lyčka, A., et al., *Inorg. Chim. Acta*, 2020, vol. 512, p. 119892.

53. Baul, T.S.B., Addepalli, M.R., Lyčka, A., et al., *J. Organomet. Chem.*, 2020, vol. 927, p. 121522.

54. Shih, Y., Ke, C., Pan, C., et al., *RSC Adv.*, 2013, vol. 3, p. 7330.

55. Salehzadeh, H. and Nematollahi, D., *RSC Adv.*, 2014, vol. 4, p. 24207.

56. Salehzadeh, H., Nematollahi, D., and Hesari, H., *Green Chem.*, 2013, vol. 15, p. 2441.

57. Lund, H. and Hammerich, O., *Organic Electrochemistry*, New York: Marcel Dekker, Inc., 2001.

58. Grusenmeyer, T.A., King, A.W., Mague, J.T., et al., *Dalton Trans.*, 2014, vol. 43, p. 17754.

59. Yenisehirli, G., Oztas, N.A., Sahin, E., et al., *Heteroat. Chem.*, 2010, vol. 21, no. 6, p. 373.

60. Smolyaninova, S.A., Poddel'sky, A.I., Smolyaninov, I.V., et al., *Russ. J. Coord. Chem.*, 2014, vol. 40, no. 5, p. 273. https://doi.org/10.1134/S107032841405011X

61. Chegerev, M.G. and Piskunov, A.V., *Russ. J. Coord. Chem.*, 2018, vol. 44, no. 4, p. 258. https://doi.org/10.1134/S1070328418040036

62. Budnikova, Y.H., Dudkina, Y.B., Kalinin, A.A., et al., *Electrochim. Acta*, 2021, vol. 368, p. 137578.

63. González-Hernandez, A., León-Negrete, A., Galván-Hidalgo, J.M., et al., *J. Mol. Struct.*, 2021, vol. 1242, p. 130807.

64. Piskunov, A.V., Trofimova, O.Y., Maleeva, A.V., and Cherkasov, A.V., *Russ. J. Coord. Chem.*, 2019, vol. 45, no. 3, p. 188. https://doi.org/10.1134/S1070328419020040

Translated by E. Yablonskaya